The Journal of Immunology

Dectin-1 Activation by a Natural Product β -Glucan Converts Immunosuppressive Macrophages into an M1-like Phenotype

Min Liu, Fengling Luo, Chuanlin Ding, Sabrin Albeituni, Xiaoling Hu, Yunfeng Ma, Yihua Cai, Lacey McNally, Mary Ann Sanders, Dharamvir Jain, Goetz Kloecker, Michael Bousamra II, Huang-ge Zhang, Richard M. Higashi, Andrew N. Lane, Teresa W.-M. Fan and Jun Yan

J Immunol published online 9 October 2015
http://www.jimmunol.org/content/early/2015/10/09/jimmunol.1501158

The Journal of Immunology is published twice each month by The American Association of Immunologists, Inc., 9650 Rockville Pike, Bethesda, MD 20814-3994.

Print ISSN: 0022-1767 Online ISSN: 1550-6606.

Published October 9, 2015, doi:10.4049/jimmunol.1501158

Dectin-1 Activation by a Natural Product β-Glucan Converts Immunosuppressive Macrophages into an M1-like Phenotype

Min Liu,*,†,[1] Fengling Luo,*,†,[1] Chuanlin Ding,*,[1] Sabrin Albeituni,‡ Xiaoling Hu,* Yunfeng Ma,* Yihua Cai,* Lacey McNally,* Mary Ann Sanders,§ Dharamvir Jain,* Goetz Kloecker,* Michael Bousamra, II,¶ Huang-ge Zhang,‡ Richard M. Higashi,‖,[2] Andrew N. Lane,*,‖,#,[2] Teresa W.-M. Fan,‖,#,[2] and Jun Yan*,‡

Tumor-associated macrophages (TAM) with an alternatively activated phenotype have been linked to tumor-elicited inflammation, immunosuppression, and resistance to chemotherapies in cancer, thus representing an attractive target for an effective cancer immunotherapy. In this study, we demonstrate that particulate yeast-derived β-glucan, a natural polysaccharide compound, converts polarized alternatively activated macrophages or immunosuppressive TAM into a classically activated phenotype with potent immunostimulating activity. This process is associated with macrophage metabolic reprograming with enhanced glycolysis, Krebs cycle, and glutamine utilization. In addition, particulate β-glucan converts immunosuppressive TAM via the C-type lectin receptor dectin-1–induced spleen tyrosine kinase–Card9–Erk pathway. Further in vivo studies show that oral particulate β-glucan treatment significantly delays tumor growth, which is associated with in vivo TAM phenotype conversion and enhanced effector T cell activation. Mice injected with particulate β-glucan–treated TAM mixed with tumor cells have significantly reduced tumor burden with less blood vascular vessels compared with those with TAM plus tumor cell injection. In addition, macrophage depletion significantly reduced the therapeutic efficacy of particulate β-glucan in tumor-bearing mice. These findings have established a new paradigm for macrophage polarization and immunosuppressive TAM conversion and shed light on the action mode of β-glucan treatment in cancer. ***The Journal of Immunology*****, 2015, 195: 000–000.**

Macrophages are the major tumor-infiltrating leukocytes and play a critical role in cancer-related inflammation (1, 2). Depending on the different activation signals, macrophages may undergo polarized activation (3). Classically activated macrophages (M1) are characterized by elevated expression of MHC class II, expression of IL-12 and TNF-α, generation of reactive oxygen species and NO, and have tumoricidal activity. In contrast, macrophages alternatively activated (M2) have potent tumor-promoting activity. Macrophage polarization is also linked to differential metabolic programming (4). In the tumor microenvironment, most macrophages have an M2-like phenotype (5); they express low levels of MHC class II, IL-12, and TNF-α while expressing high levels of vascular endothelial growth factor, arginase-1, and cyclooxygenase-2–derived PGE_2 as well as the anti-inflammatory cytokine IL-10. Tumor immune evasion has been linked to a switch from M1 activation in the early stages of tumor initiation toward an M2-like phenotype during tumor progression, a process that highlights the heterogeneity and plasticity of macrophage activation and offers a possible therapeutic target directed against repolarizing the tumor-associated macrophage (TAM) phenotype in the tumor (6, 7). Although using the M1/M2 model to describe macrophage polarization is a question of debate (7), clinical studies have demonstrated that high macrophage density correlates with poor patient prognosis (8–10). In human patients with non–small cell lung carcinoma (NSCLC), there is a strong association between poor survival and increased macrophage infiltration within the tumor microenvironment (11, 12). TAM also limit the efficacy of chemotherapeutic agents (13–15). These findings collectively suggest that targeting macrophages within the tumors may provide effective immunotherapy for cancer.

*Division of Hematology/Oncology, Department of Medicine, James Graham Brown Cancer Center, University of Louisville, Louisville, KY 40202; †Department of Immunology, Wuhan University School of Medicine, Wuhan 430072, China; ‡Department of Microbiology and Immunology, University of Louisville School of Medicine, Louisville, KY 40202; §Department of Pathology, University of Louisville School of Medicine, Louisville, KY 40202; ¶Department of Cardiovascular Thoracic Surgery, University of Louisville, Louisville, KY 40202; ‖Department of Chemistry, University of Louisville, Louisville, KY 40202; and #Center for Regulatory and Environmental Analytical Metabolomics, University of Louisville, Louisville, KY 40202

[1]M.L., F.L., and C.D. contributed equally to this work.

[2]Current address: Department of Toxicology and Markey Cancer Center, University of Kentucky, Lexington, KY.

ORCIDs: 0000-0001-7095-1344 (M.L.); 0000-0003-3482-8001 (D.J.); 0000-0003-1121-5106 (A.N.L.).

Received for publication May 19, 2015. Accepted for publication September 10, 2015.

This work was supported by National Institutes of Health Grants R01CA150947, P01CA163223, and 1U24DK097215, National Science Foundation/Experimental Program to Stimulate Competitive Research EPS-0447479, and the Kentucky Lung Cancer Research Program.

The sequences presented in this article have been submitted to the Gene Expression Omnibus (http://www.ncbi.nlm.nih.gov/geo/query/acc.cgi?acc=GSE71814) under accession number GSE71814.

Address correspondence and reprint requests to Dr. Jun Yan, Tumor Immunobiology Program, James Graham Brown Cancer Center, Clinical & Translational Research Building, Room 319, University of Louisville, 505 South Hancock Street, Louisville, KY 40202. E-mail address: jun.yan@louisville.edu

The online version of this article contains supplemental material.

Abbreviations used in this article: BMM, bone marrow–derived macrophage; ΔΔCt, change-in-threshold; FT-ICR-MS, Fourier transform ion cyclotron–mass spectrometry; GC-MS, gas chromatograph–mass spectrometry; HSQC, heteronuclear single quantum coherence; iNOS, inducible NO synthase; KO, knockout; LLC, Lewis lung carcinoma; M1, classically activated; M2, alternatively activated; NMR, nuclear magnetic resonance; NSCLC, non–small cell lung carcinoma; qRT-PCR, quantitative real-time PCR; Syk, spleen tyrosine kinase; TAM, tumor-associated macrophage; Tg, transgenic; WGP, whole glucan particle; WT, wild-type.

Natural product β-glucans have been investigated for their antitumor and anti-infective activity (16). Most β-glucans, which are derived from yeast, fungi, bacteria, or barley, have a backbone structure of linear β-1, 3-linked D-glucose subunits (β-1,3-D-glucan). As a pattern-recognition molecule, fungal β-glucans have been shown to trigger phagocytosis, generation of superoxide by the NADPH oxidase, and inflammatory cytokine production on macrophages (17–20). In addition, fungal β-glucan binds to its receptor dectin-1 to form a phagocytic synapse, thus initiating direct cellular antimicrobial responses (21). On the contrary, dectin-1 activation by fungal ligand zymosan induces regulatory macrophage phenotype (22). However, it is unknown whether β-glucan has any effect on polarized macrophages in tissues such as TAM. In addition, it is unclear whether β-glucan stimulation alters macrophage metabolism.

In this study, we demonstrated that yeast-derived particulate β-glucan treatment converts polarized M2 bone marrow–derived macrophages (BMM) and immunosuppressive TAM to an M1-like phenotype, leading to reduced tumor progression. This effect is associated with macrophage metabolic reprograming and mediated through the dectin-1–dependent canonical spleen tyrosine kinase (Syk)–Card9–Erk pathway. Further in vivo studies showed that tumor-bearing mice orally administered with particulate β-glucan had significantly reduced tumor burden with converted TAM phenotype and enhanced effector T cell activation. These findings reveal an unprecedented effect of natural compound β-glucan on immunosuppressive macrophage conversion and tumor microenvironment modulation.

Materials and Methods

Mice and in vivo tumor models

Wild-type (WT) C57BL/6 mice were purchased from the National Cancer Institute. Dectin-1 knockout (KO), CD11b KO, and Card9 KO mice were described previously (23, 24). OT-I and OT-II mice were purchased from Taconic Farms. For whole glucan particle (WGP) β-glucan treatment protocol, mice were implanted s.c. with Lewis lung carcinoma (LLC) cells (2×10^5/mouse) or EO771 cells (6×10^5/mouse). On day 8 after palpable tumors formed, mice were treated with WGP β-glucan orally (800 μg/mouse) or 100 μl PBS given every day using an intragastric gavage needle. WGP β-glucan was from Biothera (Eagan, MN). In some experiments, LLC cells were mixed with TAM (2.5:1) treated with or without WGP β-glucan and then injected into mice. For macrophage depletion protocol, mice were injected i.v. with 100 μl clodronate (5 mg/ml; Clodrosome; Encapsula NanoSciences, Brentwood, TN) 1 d prior to LLC s.c. inoculation. Mice were then injected with clodronate weekly during the experiment. Tumor diameters were measured every third day, and mice were euthanized when tumors reached 15 mm in diameter. Tumor volume was calculated by the following formula: length × width^2/2. For an in vivo imaging analysis, TAM were labeled with XenoLight DiR dye (PerkinElmer), whereas LLC were labeled with Vivo Track 680 (PerkinElmer). Mice were imaged with Spectral Ami (Spectral Instrument Imaging). The murine tumor protocols were performed in compliance with all relevant laws and institutional guidelines and approved by the Institutional Animal Care and Use Committee of the University of Louisville.

Immunohistochemistry staining and immunofluorescence staining. Formalin-fixed, paraffin-embedded human breast cancer tissue blocks corresponding to the reviewed cases were pulled from the University of Louisville's Department of Pathology archives. Five-micron sections from the formalin-fixed, paraffin-embedded tissue blocks were placed on glass slides. The slides were immunostained for anti-human CD68 (KP1; eBioscience), anti-CD163 (1:400; 10D6; Novacastra, Buffalo Grove, IL), or anti–HLA-DR (1:50; LN-3; Novacastra) via an automated system (Bond Max; Leica Microsystems, Buffalo Grove, IL) using both the DAB-Bond Polymer Refine Detection System and the Red-Bond Polymer Red Detection System (Leica Microsystems) according to the manufacturer's instructions. Appropriate positive and negative controls were used throughout the study.

Cryosections from fresh human lung cancer tissues or mouse tumor tissues were fixed with ice-cold acetone for 20 min. The slides were blocked with 5% BSA in PBS for 1 h and subjected to incubation at 4˚C overnight with the following primary Ab mixtures: biotin–anti-human CD68 (1:100), biotin–anti-CD163, Alexa Fluor 647–anti-HLA-DR (1:100), or biotin–anti-CD31 (1:100). Slides were washed and then incubated with streptavidin–Alexa Fluor 488 conjugate (1:200) or streptavidin–Alexa Fluor 594 conjugate (1:200) for 90 min. The slides were costained with DAPI and mounted with fluoro-gel (Electron Microscopy Science). Confocal images were acquired by Leica TCS SP5 confocal microscope system (Leica Microsystems) and quantitated by ImageJ software (National Institutes of Health).

Macrophage polarization and TAM purification

Bone marrow cells were isolated from the femurs and tibias and resuspended in DMEM supplemented with 10% FBS, 100 U/ml penicillin, and 100 μg/ml streptomycin. Cells were washed, counted, and then added (4×10^6) into 60 mm^2 petri dishes. GM-CSF (50 ng/ml; BD Biosciences) or M-CSF (100 ng/ml; PeproTech) was added to polarize the M1 or the M2 macrophages, respectively. The medium was changed on day 4. On day 7, adherent cells were used for the subsequent experiments. For some experiments, BM cells were cultured in complete DMEM containing 10 ng/ml M-CSF. The medium was changed on day 3, and cells were cultured for additional 3 d to generate M0 macrophages. On day 6, medium was changed with fresh DMEM containing 20 ng/ml IL-4 and IL-13. The cells were cultured for 2 d. These cells were designated as IL-4/IL-13–polarized M2 BMM.

For TAM purification, tumors (12–15 mm) were minced and then digested with buffer containing collagenase IV, hyaluronidase, and DNase-I at 37˚C for 30 min. Single-cell suspensions were separated using 60 and 30% Percoll, and the middle layer of cells was collected, washed, and resuspended in MACS running buffer. Cells were first blocked with Fc-blocking mAb for 15 min on ice and then stained with biotin–anti-mouse F4/80 Ab. The cells were washed and incubated with streptavidin microbeads on ice for 15 min. TAM were purified by AutoMACS separator (Miltenyi Biotec). These cells were CD11b$^+$F4/80^{hi}, and the purity was ≥90% as assessed by flow cytometry. In some experiments, these cells were further sorted based on Ly6C and MHC class II expression. Ly6C–MHC class II– TAM were further sorted by FACSAria III (BD Biosciences).

In vitro TAM–T cell coculture assay

TAM purified from LLC-bearing mice were treated with or without the Erk inhibitor PD98059 (30 μmol) for 2 h and then washed and stimulated with WGP for 24 h. TAM were collected and cocultured with CFSE-labeled splenocytes from OT-I or OT-II mice in the presence of OVA for 3 d. Cells were restimulated with PMA plus ionomycin for 6 h and then stained with CD4 or CD8 mAbs, fixed, and permeabilized for intracellular cytokine staining.

RNA microarray analysis and quantitative real-time PCR

RNAs were extracted from polarized M2 BMM stimulated with or without WGP β-glucan for 6 h with a Qiagen RNeasy kit (Qiagen). Agilent oligonucleotide arrays were performed and analyzed at the James Graham Brown Cancer Center Microarray core facility, University of Louisville. Complete array data were deposited in a public database (Gene Expression Omnibus; http://www.ncbi.nlm.nih.gov/geo/query/acc.cgi?acc=GSE71814). For quantitative real-time PCR (qRT-PCR) analysis, RNA samples were transcripted into cDNA with a Reverse Transcription Kit (Bio-Rad). qRT-PCR was then performed on a MyiQ single-color RT-PCR detection system with SYBR Green Supermix (Bio-Rad). Primer sequences for each gene were as follows: *IL-10*, forward: 5′-AGTGGAGCAGGTGAAGAGTG-3′, reverse: 5′-TTCGGAGAGAGGTACAAACG-3′; *Arginase*, forward: 5′-CAGAAGAATGGAAGAGTCGA-3′, reverse: 5′-CAGATATGCAGGGAGTCACC-3′; *IL-1β*, forward: 5′-CCCAACTGGTACATCAGCAC-3′, reverse: 5′-TCTGCTCATTCACGAAAAGG-3′, *IL-6*, forward: 5′-TCCCCTCCAGGAGCCCAGCTA-3′, reverse: 5′-CAGGGCTGAGATGCCGTCGAG-3′; *TNF-α*, forward: 5′-ACCCACGGCTCCACCCTCTC-3′, reverse: 5′-CCCTCTGGGGGCCGATCACT-3′; inducible NO synthase (*iNOS*), forward: 5′-AATAGAGGAACATCTGGCCAGG-3′, reverse: 5′-ATGGCCGACCTGATGTTGC-3′; *IL-12p35*, forward: 5′-CAGAATCACAACCATCAGCAG-3′, reverse: 5′-CACCCTGTTGATGGTCACGAC-3′. Gene expression was measured by the change-in-threshold (ΔΔCt), where $\Delta Ct = Ct_{\text{target gene}} - Ct_{\text{Housekeeping gene}}$, and $\Delta\Delta Ct = \Delta Ct_{\text{induced}} - \Delta Ct_{\text{reference}}$. We normalized gene expression levels to housekeeping genes as indicated.

Western blot analysis

For immunoblot analysis, BMM and TAM stimulated with or without WGP β-glucan were lysed in Triton X-100 lysis buffer containing protease and

phosphatase inhibitors. In some experiments, the Syk inhibitor piceatannol (30 μg/ml; Sigma-Aldrich) was added. The whole-cell extracts were separated by SDS-PAGE and electrotransferred to a polyvinylidene difluoride membrane. After blocking, the membranes were probed overnight at 4°C with appropriate primary Abs and then secondary Ab. The primary Abs included p-Erk1/2 (Thr^{202}/Tyr^{204}; Cell Signaling Technology), Erk1/2 (MK1; Santa Cruz Biotechnology), p-Stat3 (Tyr^{705}; Cell Signaling Technology), p-AKT (Ser^{473}; Cell Signaling Technology), p-p38 (Thr^{180}/Tyr^{182}; Cell Signaling Technology), and pZap/Syk (Tyr^{352}; Cell Signaling Technology). The blots were developed using ECL Plus Western blotting Detection Reagents (GE Healthcare).

Tracer treatment and stable isotope resolved metabolomics analyses

M2 BMM treated with or without WGP β-glucan (100 μg/ml) and M1 BMM were maintained for 25 h in DMEM supplemented with either 2 mmol $[^{13}C]_5,^{15}N_2$-Gln or 10 mmol $[^{13}C]_6$-Glc. Aliquots of the medium were taken at 0 and 25 h. The cells were rinsed in cold PBS, quenched in cold acetonitrile, extracted for metabolites, and prepared for gas chromatograph–mass spectrometry (GC-MS), Fourier transform ion cyclotron (FT-ICR)-MS, and nuclear magnetic resonance (NMR) analysis as described previously (25). NMR spectra were recorded at 14.1 T under standard acquisition conditions using 1D proton and 1D $[^{1}H]\{[^{13}C]\}$-heteronuclear single quantum coherence (HSQC) for isotopomer analysis. GC-MS was performed on a Thermo Finnigan Polaris instrument (Thermo Scientific). Peaks were assigned and quantified as previously described (25).

Flow cytometry

Single-cell suspensions were blocked in the presence of anti-CD16/CD32 for cells from mice at 4°C for 15 min and stained on ice with the appropriate Abs and isotype controls in PBS containing 1% FBS. Fluorochrome-labeled CD11b, CD45, F4/80, CD4, CD8, IFN-γ, and Foxp3 mAbs were purchased from BioLegend or eBioscience. The samples were acquired using an FACSCalibur or FACSCanto II cytometer (BD Biosciences) and analyzed using FlowJo software (Tree Star, Ashland, OR).

Statistical analysis

Data are expressed as means ± SEM. The unpaired Student *t* test was used to determine the significance of differences between M1 versus M2 or M2 plus WGP versus M2 datasets. To correct for multiple testing, the false discovery rate q values were calculated according to the formula:

$$q_i = p_i * N / rank(i),$$

where p_i is the uncorrected *p* value for the i^{th} metabolite, *N* is the number of metabolites tested, and rank (*i*) is the ordinal rank order of the *p* values. Significance was assumed to be reached at $p < 0.05$. Statistical analysis was performed using Prism 5.0 (GraphPad Software).

Results

Macrophages with the M2 phenotype are the major constitutes of leukocytes within the tumor microenvironment

Previous studies have shown that macrophage infiltration in human breast cancer and NSCLC is associated with tumor invasion and progression (9, 12). As shown in Supplemental Fig. 1A, there were abundant macrophages infiltrated within the human breast cancer tissue ($CD68^+$, brown). In humans, HLA-DR and CD163 are used to costain with CD68 to differentiate between M1 (CD68/HLA-DR double positive) and M2 macrophages (CD68/CD163 double positive) (26, 27). In human breast cancer tissues, macrophages costained with CD68 and CD163 (brown and red, respectively) but not with HLA-DR (Supplemental Fig. 1A). Similarly, we observed accumulation of macrophages with the M2 phenotype in the human NSCLC tumors (Supplemental Fig. 1B). Additionally, three murine tumor models were established including LLC, mammary carcinoma EO771, and B16 melanoma. Among $CD45^+$ leukocytes infiltrated within the tumors, $CD11b^+$ myeloid cells constituted the predominant population, and $F4/80^+$ macrophages were the significant infiltrated leukocytes (Supplemental Fig. 1C). These macrophages showed the typical M2 phenotype with potent immune suppressive function (Supplemental Fig. 1D and data not shown).

β-Glucan converts in vitro polarized M2 BMM into an M1-like phenotype via dectin-1 receptor

Because the majority of TAM is of the M2 phenotype, we first examined whether β-glucan treatment would alter the M2 macrophage phenotype. To this end, BMM were polarized into the M2 phenotype (28). We used a gene microarray to determine the gene expression changes in the M2 BMM after stimulation with yeast-derived particulate β-glucan WGP. As depicted in Fig. 1A, the expression of the conventional M2 marker genes including *Cd163*, *Mrc1*, *Il-23a*, *Fcgr*, *Ccl17*, *Ccl19*, and *Maf* were significantly downregulated upon WGP treatment. Conversely, the M1 markers, such as *Il-12*, *Ifng*, *Cd40*, and *Cd86* were upregulated after stimulation. β-Glucan treatment also decreased the mRNA levels of arginase I and IL-10, whereas it increased mRNA levels of iNOS, IL-12, TNF-α, IL-1β, and IL-6 (Fig. 1B). We also used IL-4/IL-13 protocol to polarize M2 BMM. Similarly, β-glucan treatment promoted M1 signature gene expression including iNOS, IL-12p35, TNF-α, IL-1β, and IL-6, whereas it downregulated IL-10 and arginase mRNA expression levels (data not shown). These effects were mediated through the dectin-1 pathway and independent of CD11b. Next, we examined whether β-glucan treatment alters M2-suppressive function. To this end, splenocytes from OT-I and OT-II mice were CSFE labeled and then stimulated with OVA in the presence of M2 BMM treated with or without particulate β-glucan. As shown in Fig. 1C, M2 indeed showed potent immunosuppressive activity on both CD4 and CD8 T cell proliferation. Particulate β-glucan treatment significantly abolished M2-mediated immunosuppression, suggesting that M2 macrophages are converted both phenotypically and functionally upon β-glucan in vitro treatment. In contrast, WGP treatment had minimal effect on M1 BMM (Supplemental Fig. 1E).

Previous studies have shown that the dectin-1 pathway signals via Syk kinase to recruit and activate CARD9/Bcl10 and subsequently the p65/p50 pathway and Malt1 (29). WGP stimulation induced phosphorylation of Syk, Akt, and Erk1/2 dependent of dectin-1 receptor but did not induce phosphorylation of STAT3 or p38 (Fig. 1D). To investigate whether Erk is downstream of the canonical dectin-1–Syk/Card9 pathway, the Syk inhibitor and Card9 KO BMM were used. The phosphorylation of Syk and Erk1/2 stimulated by WGP β-glucan was abolished by the Syk inhibitor, suggesting Erk phosphorylation is downstream of Syk activation (Fig. 1E). In addition, β-glucan–induced Erk phosphorylation was abolished in Card9 KO mice (Fig. 1F). These data suggest that particulate β-glucan is capable of converting M2 BMM into an M1-like phenotype via the dectin-1/Syk/Card9/Erk signaling pathway.

M1 versus M2 BMM display distinct metabolism, and β-glucan–treated M2 BMM exhibit M1-like metabolic activity

Increasing evidence indicates that macrophage activation and function are controlled by cellular metabolism (30). As the M1 and M2 macrophages are functionally distinct and may involve altered expression of genes that regulate metabolism, we thus employed the stable isotope0resolved metabolomics approach by using uniformly ^{13}C-labeled glucose ($[^{13}C]_6$-Glc) and ^{13}C-/^{15}N-labeled glutamine ($[^{13}C]_5,^{15}N_2$-Gln) as tracers, followed by NMR and MS analysis of isotopic labeling patterns of various metabolites to enable the reconstruction of altered metabolic networks induced by M2/M1 polarization and β-glucan activation (31, 32). M1 and M2 BMM exhibited distinct Glc and Gln metabolism via

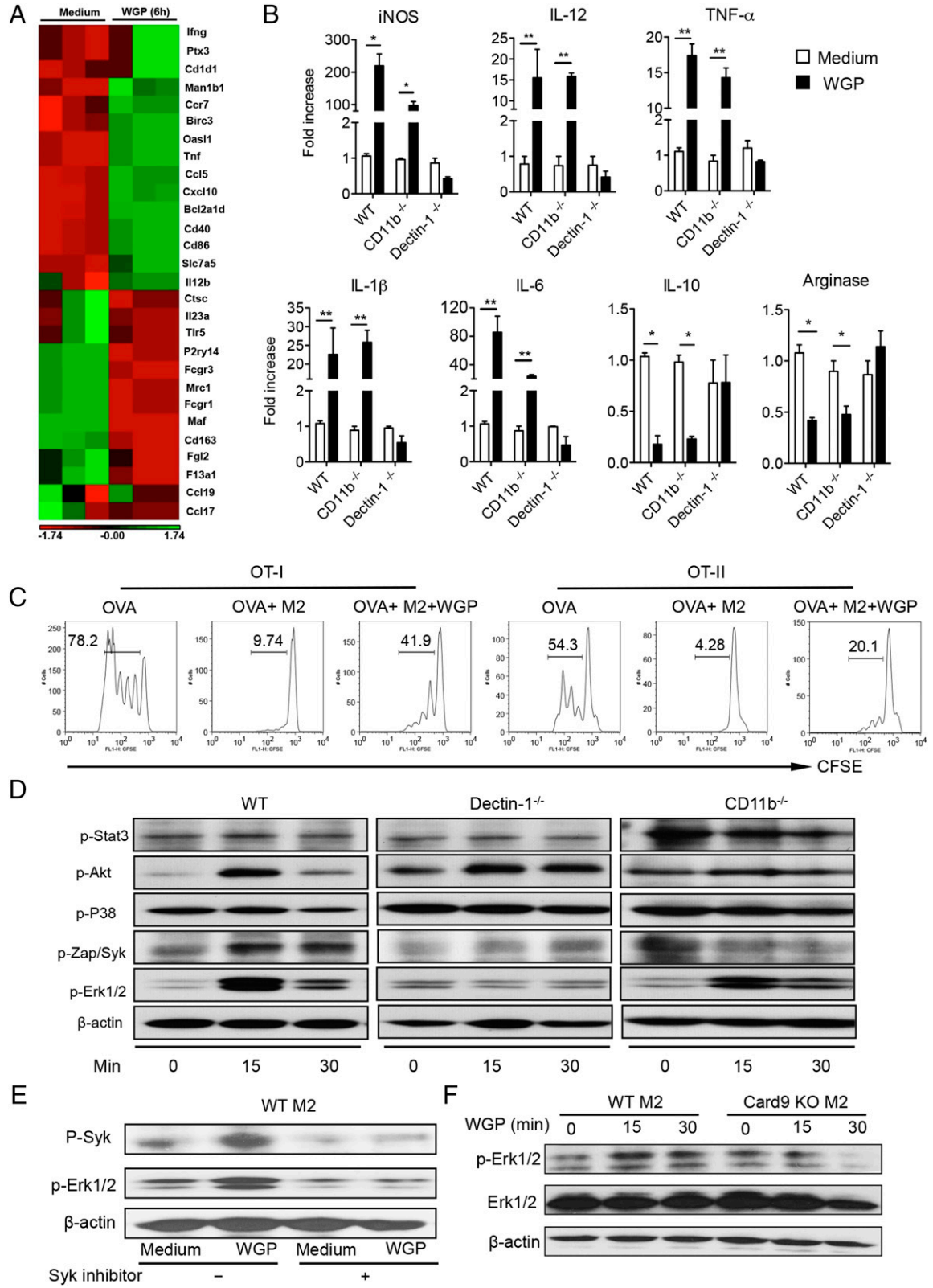

FIGURE 1. β-Glucan treatment converts M2 macrophage characteristic gene expression and its immunosuppressive function and activates Syk/Erk in a dectin-1–dependent manner. (**A**) Polarized M2 BMM from WT mice ($n = 3$) were treated with WGP β-glucan for 6 h. The total RNAs were extracted for the microarray analysis. (**B**) mRNA expression levels of specific genes as indicated in polarized M2 BMM from WT, CD11b$^{-/-}$, or dectin-1$^{-/-}$ mice upon stimulation with WGP β-glucan by qRT-PCR. (**C**) Splenocytes from OVA Tg OT-I and OT-II mice were labeled with CFSE and then stimulated with OVA in the presence of polarized M2 BMM (ratio 1:20) with or without WGP β-glucan treatment. Histogram shows cell proliferation. (**D**) Polarized M2 BMM from WT, CD11b$^{-/-}$, or dectin-1$^{-/-}$ mice were stimulated with WGP β-glucan at indicated time points. Cells were lysed, and extracted proteins were probed with Abs to p-Stat3, p-Akt, p-P38, p-Zap/Syk, p-Erk1/2, and β-actin. (**E**) M2 BMM were stimulated with WGP β-glucan in the presence or absence of the Syk inhibitor. The expression of p-Syk and p-Erk1/2 was determined by Western blot. (**F**) M2 BMM from WT or Card9 KO mice were treated with or without WGP β-glucan at indicated time points. Lysates were immunoblotted with p-Erk1/2, Erk1/2, and β-actin Abs. Data are representative of three independent experiments with similar results. *$p < 0.05$, **$p < 0.01$.

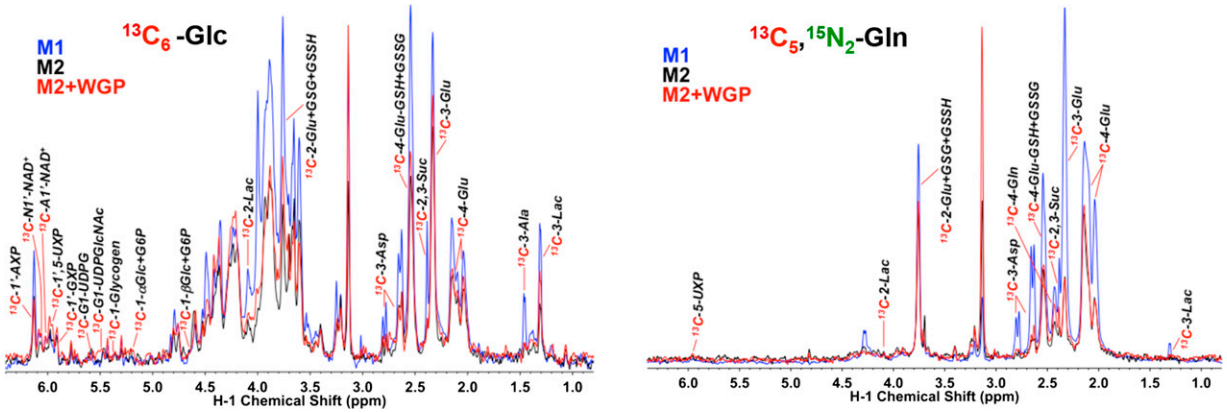

FIGURE 2. M1 and WGP β-glucan–activated M2 BMM display elevated [^{13}C] incorporation into glycolytic and Krebs cycle metabolites from labeled Glc and Gln. M1, M2, or WGP-treated M2 BMM extracts were analyzed by 1D ^{1}H{[^{13}C]} HSQC NMR as described in the *Materials and Methods*. The HSQC analysis compared the peak intensity of protons attached to [^{13}C] atoms (akin to [^{13}C] abundance) at specific positions of various metabolites. Compared to M2 BMM, M1 BMM exhibited elevated activity of glycolysis, Krebs cycle, glutathione synthesis, and nucleotide synthesis, as evidenced, respectively, by the increased [^{13}C] abundance of cellular lactate (Lac; see also Fig. 3 for medium lactate), Asp/Glu/succinate (Suc), adenine nucleotides (AXP), and glutathione (GSH)/glutathione disulfide (GSSG) derived from these pathways using Glc or Gln as precursor (Supplemental Fig. 2). WGP-treated M2 macrophages also displayed elevated activity of glycolysis and Krebs cycle over untreated M2 macrophages but not in nucleotide and glutathione biosynthesis. 1′-AXP, -GXP, and -UXP: 1′-ribose of adenine, guanine, and uracil nucleotides, respectively.

glycolysis, the Krebs cycle, the pentose phosphate pathway, and the nucleotide/glutathione/lipid biosynthetic pathways (Fig. 2). Compared to the M2 BMM, M1 exhibited elevated Glc metabolism, based on the [^{1}H] NMR analysis of increased consumption of medium [^{13}C]$_6$-Glc and increased release of triply ^{13}C-labeled lactate ([^{13}C]$_3$-Lac) into the medium; the latter indicates elevated glycolytic activity (Fig. 3A, *bottom panel*). Gln consumption was also accelerated in M1 macrophages. Subsequent [^{13}C]$_6$-Glc oxidation by the Krebs cycle and incorporation into nucleotides and glutathiones was enhanced in M1 macrophages, as revealed by the HSQC NMR analysis (Figs. 2, 3B, *top panel*). Moreover, GC-MS and FT-ICR-MS analysis of the same sets of cell extracts both corroborated and complemented the NMR analysis in revealing enhanced pentose phosphate pathway/nucleotide biosynthesis activity (Fig. 3B, *middle two panels*) and increased lipid biosynthesis (Fig. 3B, *bottom panel*) as well as enhanced oxidation of [^{13}C]$_5$,^{15}N$_2$-Gln via glutaminase and the Krebs cycle (Fig. 3C, *top panel*, Supplemental Fig. 2 for pathway tracing). These metabolic activation events are consistent with a higher capacity of M1 macrophages for expansion, as evidenced by their elevated protein levels (Fig. 3A, *top panel*) and essential amino acid content (Fig. 3C, *bottom panel*). Although WGP β-glucan treatment did not stimulate M2 macrophage proliferation, it activated many of the metabolic events as occurring in M1 macrophages (Fig. 3A–C). In addition, the accumulation of arginine in M1 and WGP β-glucan–treated M2 BMM (Fig. 3C, *bottom panel*) is consistent with the suppression of arginase in these macrophages (Fig. 1B). Thus, it is likely that these events are important to M1 activation or converting the immunosuppressive property of M2 macrophages by β-glucan.

β-Glucan treatment repolarizes immunosuppressive TAM phenotypically and functionally

We next analyzed whether β-glucan treatment is capable of modulating TAM to reverse their immunosuppressive activity. F4/80^{hi} TAM obtained from LLC-bearing mice (WT and dectin-1$^{-/-}$) were stimulated with WGP β-glucan. Similar to polarized M2 BMM, β-glucan treatment significantly downregulated the mRNA levels of arginase and IL-10, whereas it upregulated the mRNA levels of iNOS, IL-12, TNF-α, IL-1β, and IL-6 in a dectin-1 receptor–dependent manner (Fig. 4A). Because TAM are heterogeneous populations, we further sorted F4/80^{+}MHC class II^{-}Ly6C^{-}CD11b^{+} programmed cell death ligand-1^{lo} TAM, which previously were shown to be associated with enhanced M2 marker gene expression (33). WGP treatment significantly decreased the mRNA levels of IL-10 and arginase, whereas it upregulated iNOS, IL-12, TNF-α, IL-1β, and IL-6 mRNA expression levels (Supplemental Fig. 3). In addition, WGP stimulated Erk1/2 phosphorylation via the dectin-1 receptor (Fig. 4B). To further study the Erk signaling pathway in β-glucan–mediated TAM repolarization, TAM were treated with or without Erk inhibitor in the presence of WGP β-glucan treatment. The mRNA levels of TNF-α, IL-6, IL-10, and arginase were significantly affected by the Erk inhibitor treatment (Fig. 4C). However, the Erk inhibitor did not show any effect on IL-12 mRNA expression levels.

To determine the functional activity of β-glucan–treated TAM, TAM treated with or without WGP β-glucan were cocultured with CFSE-labeled splenocytes from OVA CD4 or CD8 TCR-transgenic (Tg) mice. As depicted in Fig. 4D, TAM significantly inhibited IFN-γ production by CD4 and CD8 T cells. β-Glucan in vitro treatment completely abrogated TAM-induced CD4 and CD8 T cell suppression and even induced augmented CD4 and CD8 T cell proliferation and IFN-γ production as compared with the Ag alone–stimulated CD4 and CD8 T cell responses (Fig. 4D). The Erk inhibitor completely abrogated β-glucan–induced CD4 T cell response, whereas it partly inhibited CD8 T cell activation. Taken together, these data suggest that particulate β-glucan WGP not only converts TAM phenotypically but also alters TAM functionally to induce potent Ag-specific T cell responses partly via the dectin-1–Erk pathway.

WGP β-glucan in vivo treatment reduces tumor burden and polarizes the TAM phenotype

To determine the in vivo effect of β-glucan treatment on TAM-polarized activation, tumor-bearing mice were daily administered orally either with PBS or WGP. Mice treated with WGP had a significantly decreased tumor burden compared with the mice treated with PBS (Fig. 5A, 5C). We next analyzed the phenotype of freshly isolated TAM. In the LLC tumor model, the mRNA level of arginase in TAM was significantly decreased in β-glucan–treated mice, whereas the mRNA levels of IL-12, TNF-α, and IL-6 were significantly increased (Fig. 5B). The mRNA level of IL-10

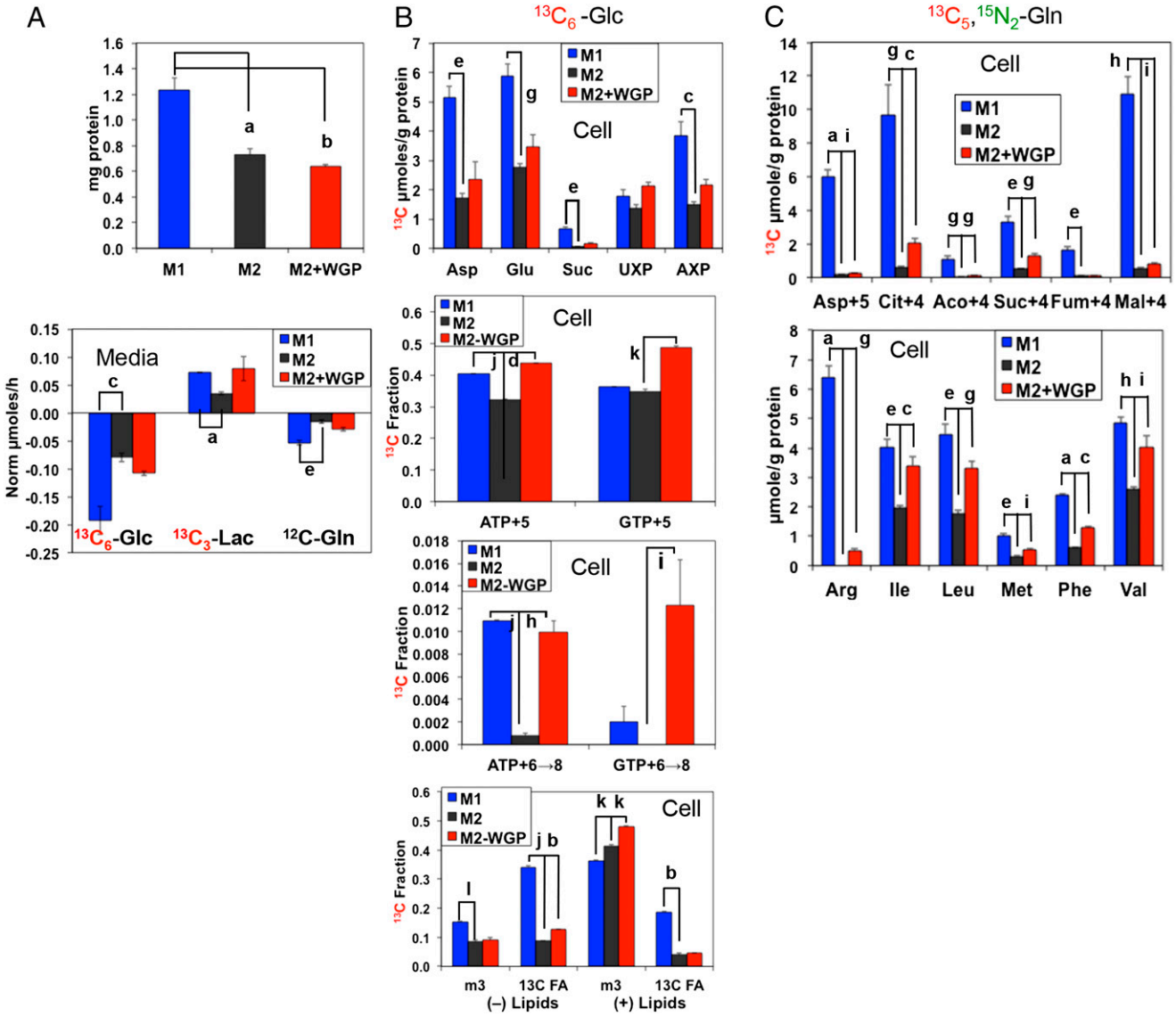

FIGURE 3. Glycolysis, Krebs cycle, and associated anabolic activities are enhanced in M1 and β-glucan–activated M2 macrophages. M1, M2, or WGP-treated M2 BMM were cocultured with labeled tracers, and the polar extracts of both cells and media prepared before analysis by 1D ^{1}H NMR (**A**, *bottom panel*), ^{1}H{[^{13}C]} HSQC NMR (**B**, *top panel*), GC-MS (**C**), and FT-ICR-MS (B, *bottom three panels*), as described in the *Materials and Methods*. The total soluble proteins were also analyzed in these cells (A, *top panel*). The medium metabolite data were calculated as micromoles per hour and normalized to that of Val, the HSQC and GC-MS quantification of cellular metabolites was expressed as micromoles per gram protein, and the FT-ICR-MS data were calculated as fraction of the total metabolite level. ATP+5 and GTP+5 represent [^{13}C]$_5$-isotopologues of ATP and GTP (i.e., fully ^{13}C-labeled in the ribose unit); ATP+6→8 and GTP+6→8 represent [^{13}C]$_{6\to8}$-isotopologues of ATP and GTP (i.e., fully ^{13}C-labeled in the ribose unit plus 1-3 [^{13}C] in the ring); m3 and [^{13}C] fatty acid (FA) are lipids containing [^{13}C]$_3$ (fully ^{13}C-labeled glycerol backbone) and ^{13}C-labeled fatty acyl chains, respectively; Asp+5, Cit+4, Aco+4, Suc+4, Fum+4, and Mal+4 are, respectively, the [^{13}C]$_4$,^{15}N$_1$ isotopologue of Asp and the [^{13}C]$_4$ isotopologues of citrate, *cis*-aconitate, succinate, fumarate, and malate. Fractional enrichment in [^{13}C] FA of lipids was obtained by summing the fractions of lipid isotopologues with even number (FA only) and >3 odd numbers (FA + glycerol backbone) of [^{13}C] atoms; (−) charged lipids include phosphatidylserines, phosphatidylglycerols, and phosphatidylinositols, whereas (+) lipids are composed of phosphatidylethanolamines, phosphatidylcholines, plasmalogens of phosphatidylethanolamines and phosphatidylcholines, sphingomyelins, and triacylglycerides. Data for M1 versus M2 or M2 + WGP versus M2 were statistically compared using unpaired *t* test with correction for false discovery rate (*q* values). a, $q \leq 0.0005$; b, $q \leq 0.0001$; c, $q < 0.02$; d, $q < 0.00001$; e, $q < 0.005$; f, $q < 0.00002$; g, $q \leq 0.01$; h, $q < 0.002$; i, $q \leq 0.05$; j, $q < 0.000005$; k, $q \leq 0.001$; and l, $q < 0.0002$.

showed decreasing trend in TAM of WGP-treated mice. Similarly, the mRNA levels of IL-12, TNF-α, and IL-6 in TAM significantly increased in EO771 tumor model upon β-glucan treatment (Fig. 5D), although the mRNA levels of arginase and IL-10 were not significantly altered. We further examined T cell responses in these mice and found that the frequency of CD4$^+$Foxp3$^+$regulatory T cells both in tumor and spleen tended to decrease in WGP-treated mice, whereas IFN-γ–producing CD4 T cells were significantly increased (Supplemental Fig. 4A). WGP treatment also significantly promoted CD8$^+$ IFN-γ–producing T cells in the tumor milieu (Supplemental Fig. 4B). These results suggest that the antitumor efficacy of β-glucan could be mediated via its effect on the TAM.

To further support this notion, we mixed LLC tumor cells with TAM treated with or without β-glucan and then injected into mice. Mice injected with LLC plus TAM had significant tumor progression as compared with tumors in mice injected with LLC and β-glucan–treated TAM (Fig. 5E). This was also shown by an

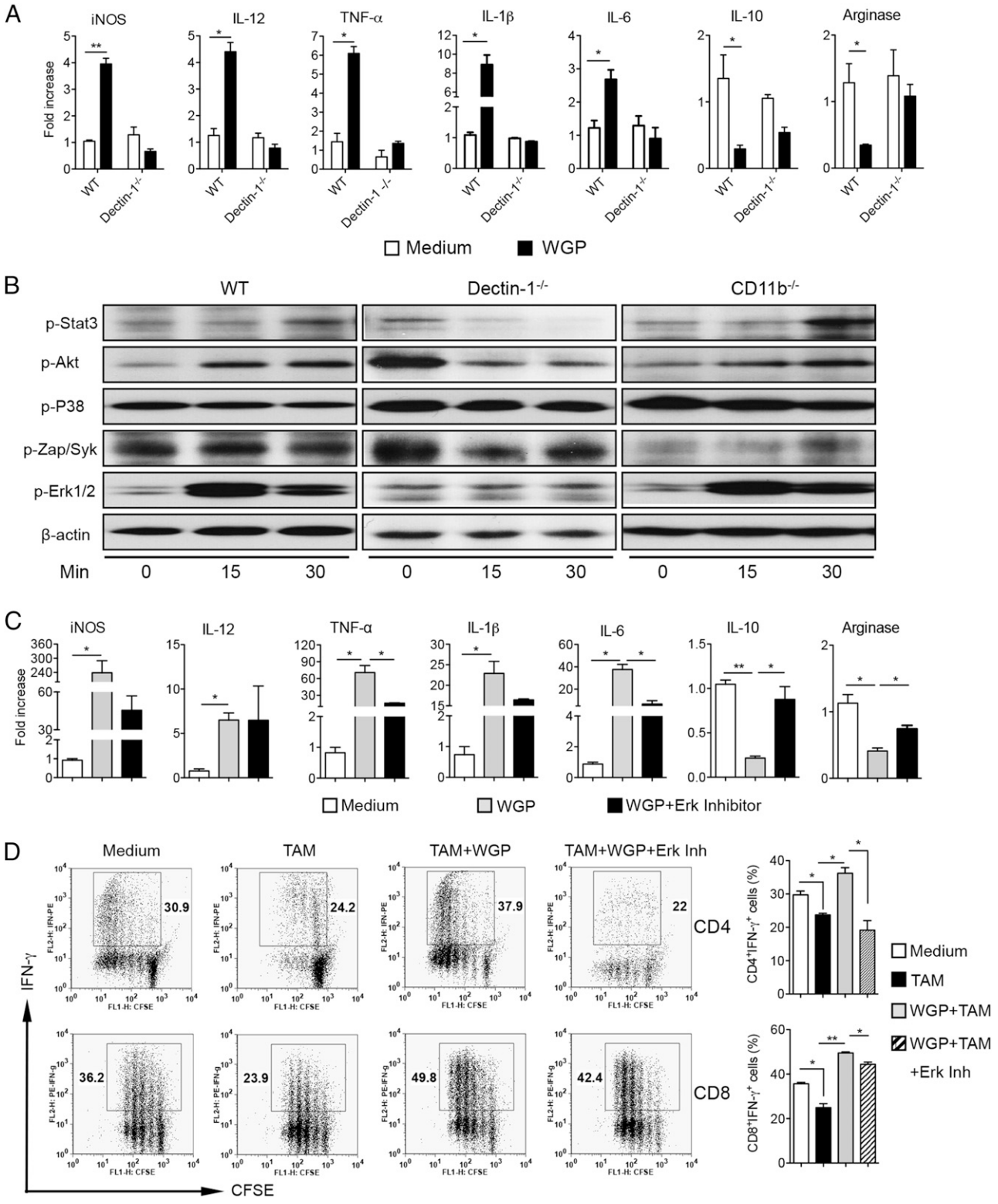

FIGURE 4. WGP β-glucan treatment alters TAM phenotype and immunosuppressive activity on T cell responses partly through the dectin-1–Erk pathway. (**A**) TAM purified from LLC tumors in WT or dectin-1 KO mice were stimulated with WGP β-glucan (150 μg/ml) for 24 h. Total RNAs were extracted, and qRT-PCR analysis was performed. (**B**) TAM from LLC-tumor bearing WT, dectin-$1^{-/-}$, or $CD11b^{-/-}$ mice were stimulated with WGP β-glucan at indicated time points. Cells were lysed, and extracted proteins were probed with Abs to p-Stat3, p-Akt, p-P38, p-Zap/Syk, p-Erk1/2, and β-actin. Data are representative of three experiments. (**C**) TAM purified from LLC-bearing mice were treated with or without the Erk inhibitor PD98059 for 2 h and then stimulated with WGP β-glucan for 24 h. RNAs were extracted, and qRT-PCR was performed for the indicated genes. (**D**) TAM isolated from LLC-bearing mice were treated with or without Erk inhibitor PD98059 for 2 h and then stimulated with WGP β-glucan for 24 h. Cells were harvested and cocultured with CFSE-labeled splenocytes from CD4 or CD8 OVA Tg mice in the presence of OVA. Splenocytes alone with the Erk inhibitor were used as controls. Graphs show CFSE dilution versus intracellular IFN-γ on day 3 of culture. Percent of $CD4^+IFN\text{-}\gamma^+$ or $CD8^+IFN\text{-}\gamma^+$ cells is shown. $*p < 0.05$, $**p < 0.01$.

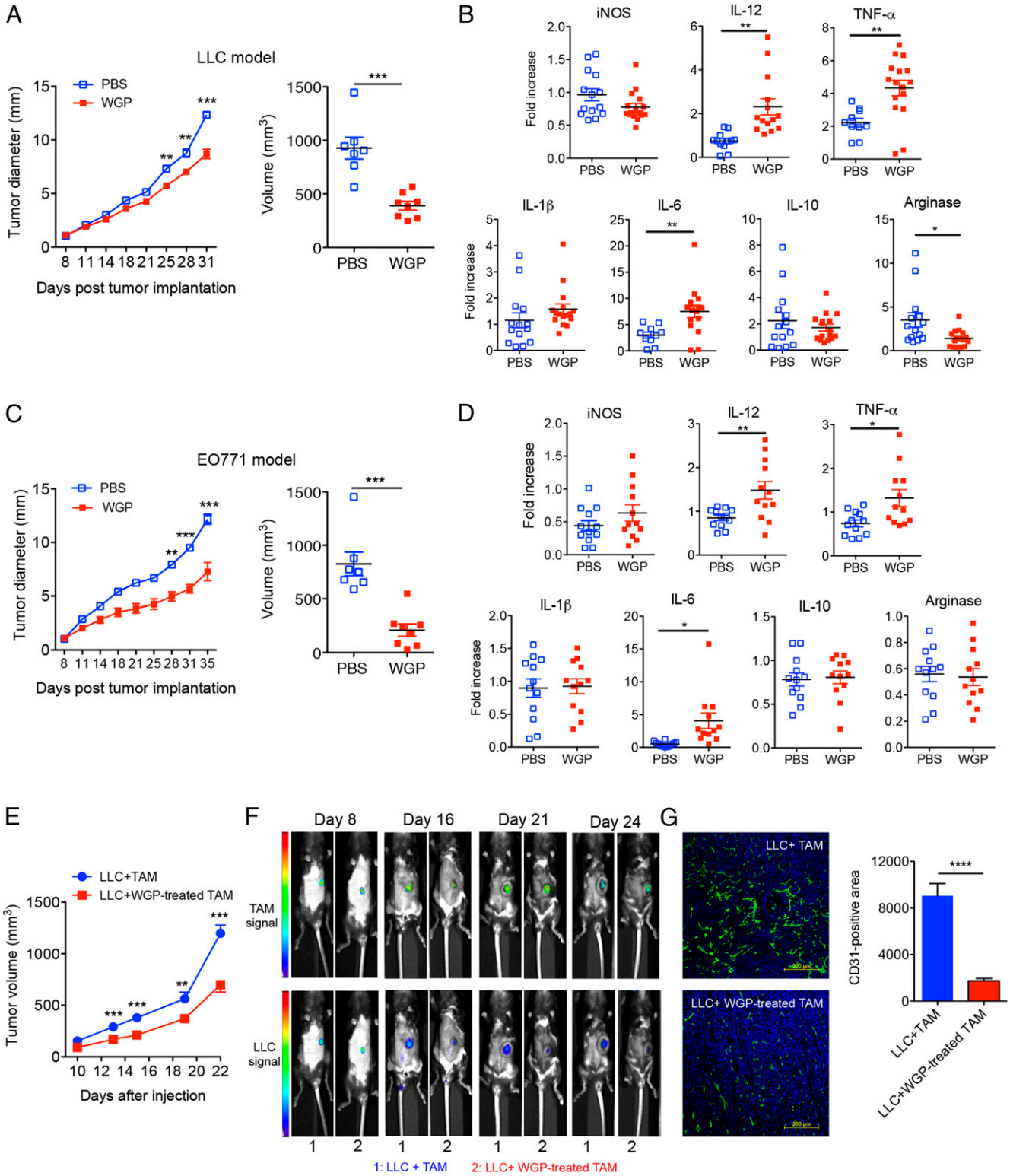

FIGURE 5. WGP β-glucan treatment significantly reduces tumor burden with altered TAM phenotype. (**A**) Groups of WT mice ($n = 7, 8$) were implanted s.c. with LLC tumor cells. When tumors were palpable, mice were fed with WGP β-glucan or PBS control for 3 wk. Tumor diameter was recorded at the indicated time. Tumor volumes for the last time point were also shown. (**B**) TAM purified from LLC tumor-bearing mice treated with or without WGP β-glucan from two independent protocols were assayed for specific gene mRNA expression levels determined by qRT-PCR. Each dot corresponds to one TAM sample sorted from one tumor. (**C**) Groups of WT mice ($n = 7, 8$) were implanted s.c. with EO771/OVA tumor cells. After palpable tumors formed, mice were treated daily with or without WGP β-glucan for 3 wk. Tumor diameter was recorded at the indicated time. Tumor volumes for the last time point were also shown. (**D**) TAM isolated from EO771-tumor bearing mice treated with or without WGP β-glucan from two independent protocols were assayed for specific gene mRNA expression levels determined by qRT-PCR. (**E**) TAM treated with or without WGP β-glucan were mixed with LLC tumor cells and then injected into mice ($n = 6, 7$). Tumor progression was monitored. (**F**) Tumor-bearing mice were imaged for tumor or TAM signals using different wavelengths at indicated time points. (**G**) Tumors from LLC plus TAM treated with or without WGP β-glucan were sectioned and stained with anti-CD31 (green) and DAPI to reveal nuclei. $CD31^+$ areas ($n = 6$) were quantitated by ImageJ software (National Institutes of Health). Scale bars, 200 μm. $^*p < 0.05$, $^{**}p < 0.01$, $^{***}p < 0.001$, $^{****}p < 0.0001$.

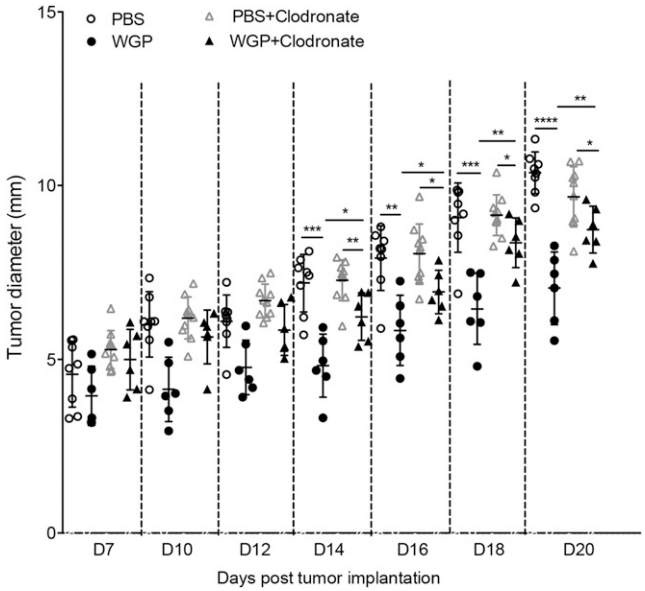

FIGURE 6. Depletion of macrophages significantly reduces WGP β-glucan–mediated therapeutic efficacy. Groups of C57BL/6 mice (n = 6–8) were injected i.v. with 100 μl clodronate (5 mg/ml) 1 d prior to LLC s.c. inoculation. Mice were then injected with clodronate weekly during the experiment. Mice without clodronate injection were used as controls. When the tumor sizes reached 5 mm in diameter, mice were treated with WGP β-glucan or control PBS daily via oral gavage. Tumor diameters were measured every other day, and mice were euthanized when tumors reached 15 mm in diameter. $*p < 0.05$, $**p < 0.01$, $***p < 0.001$, $****p < 0.0001$.

in vivo imaging analysis (Fig. 5F). We also observed that tumors from LLC plus TAM had more vascular structure as revealed by CD31 staining (Fig. 5G). Because previous studies have shown that particulate β-glucan treatment also activates dendritic cells and reverses myeloid-derived suppressor cells (23, 34), we thus examined the relative contribution of TAM conversion in the setting of β-glucan treatment by depleting macrophages. Mice were injected with clodronate to deplete macrophages prior tumor inoculation. As shown in Fig. 6, tumor-bearing mice received WGP treatment showed significant reduced tumor progression regardless of macrophage depletion. However, mice with macrophage depletion showed significant increased tumor burden upon WGP treatment compared with those without macrophage depletion (Fig. 6). Overall, these results are consistent with the view that converting TAM phenotype and function is, at least in part, responsible for the antitumor activity of β-glucan.

Discussion

Macrophages can be polarized into extreme M1 or M2 phenotype depending on the environmental cues. Although macrophage phenotype within the tumor microenvironment is more complicated, it is clear that TAM phenotypically more resemble M2 macrophages with potent immunosuppressive activity, thus representing attractive targets for cancer immunotherapeutics (35, 36). However, efforts to steer TAM functions are still in their infancy (37). Currently, strategies to target TAM include depletion or blocking of recruitment (38–40) and decreasing M2-like TAM via re-education (41–43). These approaches employ chemotherapeutic drugs, Abs, or small-molecule inhibitors, which may cause unwanted adverse effects. In addition, some of these approaches may impact all macrophage subsets including M1-like macrophages. In this study, we showed that a natural product yeast-derived β-glucan treatment converts the immunosuppressive M2 and TAM toward the M1 antitumor phenotype. Particulate β-glucan can be administered orally with proven safety profile and low cost.

We found that in vitro treatment of M2 BMM with β-glucan reverses M2 phenotype characterized as increased expression of IL-12, iNOS, TNF-α, IL-6, and IL-1β and downregulation of IL-10 and arginase in mice. This is regardless of different M2 polarization protocols. In addition, this conversion is accompanied by metabolic reprogramming to the M1 metabotype, particularly in terms of enhanced glycolysis, Krebs cycle, and glutamine utilization, which can fuel both energy and anabolic demands for activating macrophages. Although a previous study showed that macrophages with different activation signals exhibited different metabolic profiles using a [1,2-[^{13}C]$_2$]glucose tracer-based metabolomics approach (44), our studies demonstrated that glutamine uptake and subsequent metabolism to glucose and glutathione were enhanced when M2 BMM were converted into an M1-like phenotype using the stable isotope-resolved metabolomics technology. Stable isotope tracing at the atomic level enables the determination of the flow of atoms and groups of atoms from a precursor such as [^{13}C]glucose or [^{13}C], [^{15}N]glutamine through metabolic pathways, thereby discriminating which branches of a pathway differ between different cells such as M1 versus M2 macrophages. We found that glycolysis and associated anabolic activities are enhanced in M1 and β-glucan–activated M2 BMM. As tumor cells are the major nutrient consumer within the tumor microenvironment (45), this limits nutrients for other cells such as macrophages. This may be one of the mechanisms by which tumors polarize TAM into M2-like phenotype. Indeed, a recent study showed that lactic acid secreted by tumors via anaerobic glycolysis induces M2-like TAM (46).

Similarly, we demonstrated that immunosuppressive TAM from tumor-bearing mice are also phenotypically and functionally altered upon β-glucan treatment. We showed that TAM-mediated inhibition of CD4 and CD8 T cell responses is completely reversed upon β-glucan treatment in vitro. Further in vivo studies demonstrate that β-glucan treatment significantly decreases tumor burden and alters TAM phenotype, which correlates with more IFN-γ production by T cells and less regulatory T cell infiltration. It is worth noting that TAM contain heterogeneous populations, and the relative percentage of different TAM subsets changes as tumor progresses (33). Clearly, we showed that β-glucan treatment significantly alters M2-like TAM phenotypically and functionally. However, it needs further investigation whether different subsets of TAM could be differentially affected by β-glucan treatment.

C-type lectin receptor dectin-1 has been identified as the main receptor for particulate β-glucan binding and signaling (29). We showed that WGP β-glucan–mediated M2 and TAM conversion is dependent on the dectin-1 receptor. Upon β-glucan stimulation, dectin-1 can directly recruit and activate Syk kinase (47, 48). Subsequently, Syk triggers Card9 recruitment to form Card9/Bcl10/Malt-1 complex that activates the IκB kinase complex for NF-κB signaling (29). We found that the Erk inhibition partly abolishes β-glucan–mediated TAM phenotype conversion. Interestingly, glucose assumption and lactate production in macrophages are also associated with the Erk1/2 signaling (49). Although the Erk inhibitor completely abrogates β-glucan–treated TAM-mediated CD4 T cell proliferation and IFN-γ production, CD8 T cell activation is only partially affected by the Erk inhibitor, suggesting differential TAM cytokine profiles regulated by the dectin-1–Erk signaling. Previous studies have demonstrated that the dectin-1 signaling activates p38, Erk, and JNK cascade and NFAT (50, 51). Although activation of p38 and JNK via the receptor nucleotide-binding oligomerization domain 2 has been

associated with Card9 (52), it is unknown whether Erk activation is dependent on Card9. We showed that Erk phosphorylation induced by β-glucan is dependent on Card9, as Erk activation by β-glucan is completely abolished in Card9-deficient mice. These data suggest that the canonical dectin-1–Syk–Card9–Erk pathway is partially involved in β-glucan–mediated M2 BMM and TAM conversion. It still needs to be explored whether other pathway(s) is involved in this effect.

Previous studies have shown that β-glucan treatment activates dendritic cells (23) or reduces myeloid-derived suppressor cells (34) in tumor-bearing mice, thus eliciting enhanced antitumor immune responses. Because TAM are the major constitutes within the tumor milieu, findings that β-glucan treatment converts TAM immunosuppressive function are significant. Indeed, we found that macrophage depletion in tumor-bearing mice significantly reduced β-glucan–mediated antitumor therapeutic efficacy. There are several important clinical implications of this study. First, our data have established a new paradigm for macrophage polarization and immunosuppressive TAM conversion by a natural compound, β-glucan. As TAM limit chemotherapeutic drug efficacy, oral β-glucan administration can be used as immunoadjuvant therapy for patients with cancer to modulate TAM phenotype and then be combined with chemotherapeutic agents. This may turn chemoresistant tumors into chemosensitive status. Second, because TAM are an important player in establishing tumor immunosuppressive network, targeting TAM by β-glucan will provide additional benefit to improve the efficacy of other cancer immunotherapies such as adoptive T cell therapy or cancer vaccines. Collectively, this study provides a novel way to engage immunosuppressive TAM for maximizing cancer therapeutic efficacy.

Acknowledgments

We thank J. Tan and R. Balasubramaniam for performing protein measurement and assistance in the GC-MS analysis.

Disclosures

J.Y. declares a competing financial interest in Biothera, which provided β-glucan for the study. The other authors have no financial conflicts of interest.

References

1. Mantovani, A. 2009. Cancer: Inflaming metastasis. *Nature* 457: 36–37.
2. Pollard, J. W. 2009. Trophic macrophages in development and disease. *Nat. Rev. Immunol.* 9: 259–270.
3. Ruffell, B., N. I. Affara, and L. M. Coussens. 2012. Differential macrophage programming in the tumor microenvironment. *Trends Immunol.* 33: 119–126.
4. Ganeshan, K., and A. Chawla. 2014. Metabolic regulation of immune responses. *Annu. Rev. Immunol.* 32: 609–634.
5. Qian, B. Z., and J. W. Pollard. 2010. Macrophage diversity enhances tumor progression and metastasis. *Cell* 141: 39–51.
6. Mantovani, A., and A. Sica. 2010. Macrophages, innate immunity and cancer: balance, tolerance, and diversity. *Curr. Opin. Immunol.* 22: 231–237.
7. Murray, P. J., J. E. Allen, S. K. Biswas, E. A. Fisher, D. W. Gilroy, S. Goerdt, S. Gordon, J. A. Hamilton, L. B. Ivashkiv, T. Lawrence, et al. 2014. Macrophage activation and polarization: nomenclature and experimental guidelines. *Immunity* 41: 14–20.
8. Bingle, L., N. J. Brown, and C. E. Lewis. 2002. The role of tumour-associated macrophages in tumour progression: implications for new anticancer therapies. *J. Pathol.* 196: 254–265.
9. Campbell, M. J., N. Y. Tonlaar, E. R. Garwood, D. Huo, D. H. Moore, A. I. Khramtsov, A. Au, F. Baehner, Y. Chen, D. O. Malaka, et al. 2011. Proliferating macrophages associated with high grade, hormone receptor negative breast cancer and poor clinical outcome. *Breast Cancer Res. Treat.* 128: 703–711.
10. Dannenmann, S. R., J. Thielicke, M. Stöckli, C. Matter, L. von Boehmer, V. Cecconi, T. Hermanns, L. Hefermehl, P. Schraml, H. Moch, et al. 2013. Tumor-associated macrophages subvert T-cell function and correlate with reduced survival in clear cell renal cell carcinoma. *OncoImmunology* 2: e23562.
11. Chung, F. T., K. Y. Lee, C. W. Wang, C. C. Heh, Y. F. Chan, H. W. Chen, C. H. Kuo, P. H. Feng, T. Y. Lin, C. H. Wang, et al. 2012. Tumor-associated macrophages correlate with response to epidermal growth factor receptor-tyrosine kinase inhibitors in advanced non-small cell lung cancer. *Int. J. Cancer* 131: E227–E235.
12. Wang, R., J. Zhang, S. Chen, M. Lu, X. Luo, S. Yao, S. Liu, Y. Qin, and H. Chen. 2011. Tumor-associated macrophages provide a suitable microenvironment for non-small lung cancer invasion and progression. *Lung Cancer* 74: 188–196.
13. De Palma, M., and C. E. Lewis. 2011. Cancer: Macrophages limit chemotherapy. *Nature* 472: 303–304.
14. DeNardo, D. G., D. J. Brennan, E. Rexhepaj, B. Ruffell, S. L. Shiao, S. F. Madden, W. M. Gallagher, N. Wadhwani, S. D. Keil, S. A. Junaid, et al. 2011. Leukocyte complexity predicts breast cancer survival and functionally regulates response to chemotherapy. *Cancer Discov.* 1: 54–67.
15. Ruffell, B., D. Chang-Strachan, V. Chan, A. Rosenbusch, C. M. Ho, N. Pryer, D. Daniel, E. S. Hwang, H. S. Rugo, and L. M. Coussens. 2014. Macrophage IL-10 blocks CD8+ T cell-dependent responses to chemotherapy by suppressing IL-12 expression in intratumoral dendritic cells. *Cancer Cell* 26: 623–637.
16. Liu, J., L. Gunn, R. Hansen, and J. Yan. 2009. Combined yeast-derived beta-glucan with anti-tumor monoclonal antibody for cancer immunotherapy. *Exp. Mol. Pathol.* 86: 208–214.
17. Brown, G. D., J. Herre, D. L. Williams, J. A. Willment, A. S. Marshall, and S. Gordon. 2003. Dectin-1 mediates the biological effects of beta-glucans. *J. Exp. Med.* 197: 1119–1124.
18. Steele, C., L. Marrero, S. Swain, A. G. Harmsen, M. Zheng, G. D. Brown, S. Gordon, J. E. Shellito, and J. K. Kolls. 2003. Alveolar macrophage-mediated killing of *Pneumocystis carinii* f. sp. muris involves molecular recognition by the Dectin-1 beta-glucan receptor. *J. Exp. Med.* 198: 1677–1688.
19. Gantner, B. N., R. M. Simmons, S. J. Canavera, S. Akira, and D. M. Underhill. 2003. Collaborative induction of inflammatory responses by dectin-1 and Toll-like receptor 2. *J. Exp. Med.* 197: 1107–1117.
20. Goodridge, H. S., A. J. Wolf, and D. M. Underhill. 2009. Beta-glucan recognition by the innate immune system. *Immunol. Rev.* 230: 38–50.
21. Goodridge, H. S., C. N. Reyes, C. A. Becker, T. R. Katsumoto, J. Ma, A. J. Wolf, N. Bose, A. S. Chan, A. S. Magee, M. E. Danielson, et al. 2011. Activation of the innate immune receptor Dectin-1 upon formation of a 'phagocytic synapse'. *Nature* 472: 471–475.
22. Elcombe, S. E., S. Naqvi, M. W. Van Den Bosch, K. F. MacKenzie, F. Cianfanelli, G. D. Brown, and J. S. Arthur. 2013. Dectin-1 regulates IL-10 production via a MSK1/2 and CREB dependent pathway and promotes the induction of regulatory macrophage markers. *PLoS One* 8: e60086.
23. Qi, C., Y. Cai, L. Gunn, C. Ding, B. Li, G. Kloecker, K. Qian, J. Vasilakos, S. Saijo, Y. Iwakura, et al. 2011. Differential pathways regulating innate and adaptive antitumor immune responses by particulate and soluble yeast-derived β-glucans. *Blood* 117: 6825–6836.
24. Wu, W., Y. M. Hsu, L. Bi, Z. Songyang, and X. Lin. 2009. CARD9 facilitates microbe-elicited production of reactive oxygen species by regulating the LyGDI-Rac1 complex. *Nat. Immunol.* 10: 1208–1214.
25. Le, A., A. N. Lane, M. Hamaker, S. Bose, A. Gouw, J. Barbi, T. Tsukamoto, C. J. Rojas, B. S. Slusher, H. Zhang, et al. 2012. Glucose-independent glutamine metabolism via TCA cycling for proliferation and survival in B cells. *Cell Metab.* 15: 110–121.
26. Ma, J., L. Liu, G. Che, N. Yu, F. Dai, and Z. You. 2010. The M1 form of tumor-associated macrophages in non-small cell lung cancer is positively associated with survival time. *BMC Cancer* 10: 112.
27. Heusinkveld, M., P. J. de Vos van Steenwijk, R. Goedemans, T. H. Ramwadhdoebe, A. Gorter, M. J. Welters, T. van Hall, and S. H. van der Burg. 2011. M2 macrophages induced by prostaglandin E2 and IL-6 from cervical carcinoma are switched to activated M1 macrophages by CD4+ Th1 cells. *J. Immunol.* 187: 1157–1165.
28. Krausgruber, T., K. Blazek, T. Smallie, S. Alzabin, H. Lockstone, N. Sahgal, T. Hussell, M. Feldmann, and I. A. Udalova. 2011. IRF5 promotes inflammatory macrophage polarization and TH1-TH17 responses. *Nat. Immunol.* 12: 231–238.
29. Sancho, D., and C. Reis e Sousa. 2012. Signaling by myeloid C-type lectin receptors in immunity and homeostasis. *Annu. Rev. Immunol.* 30: 491–529.
30. Través, P. G., P. de Atauri, S. Marín, M. Pimentel-Santillana, J. C. Rodríguez-Prados, I. Marín de Mas, V. A. Selivanov, P. Martín-Sanz, L. Boscá, and M. Cascante. 2012. Relevance of the MEK/ERK signaling pathway in the metabolism of activated macrophages: a metabolomic approach. *J. Immunol.* 188: 1402–1410.
31. Fan, T. W., A. N. Lane, R. M. Higashi, M. A. Farag, H. Gao, M. Bousamra, and D. M. Miller. 2009. Altered regulation of metabolic pathways in human lung cancer discerned by (13)C stable isotope-resolved metabolomics (SIRM). *Mol. Cancer* 8: 41.
32. Fan, T. W., A. N. Lane, R. M. Higashi, and J. Yan. 2011. Stable isotope resolved metabolomics of lung cancer in a SCID mouse model. *Metabolomics* 7: 257–269.
33. Movahedi, K., D. Laoui, C. Gysemans, M. Baeten, G. Stangé, J. Van den Bossche, M. Mack, D. Pipeleers, P. In't Veld, P. De Baetselier, and J. A. Van Ginderachter. 2010. Different tumor microenvironments contain functionally distinct subsets of macrophages derived from Ly6C(high) monocytes. *Cancer Res.* 70: 5728–5739.
34. Tian, J., J. Ma, K. Ma, H. Guo, S. E. Baidoo, Y. Zhang, J. Yan, L. Lu, H. Xu, and S. Wang. 2013. β-Glucan enhances antitumor immune responses by regulating differentiation and function of monocytic myeloid-derived suppressor cells. *Eur. J. Immunol.* 43: 1220–1230.
35. Noy, R., and J. W. Pollard. 2014. Tumor-associated macrophages: from mechanisms to therapy. [Published erratum appears in 2014 *Immunity* 41: 866.] *Immunity* 41: 49–61.

36. Mantovani, A., and P. Allavena. 2015. The interaction of anticancer therapies with tumor-associated macrophages. *J. Exp. Med.* 212: 435–445.
37. Bronte, V., and P. J. Murray. 2015. Understanding local macrophage phenotypes in disease: modulating macrophage function to treat cancer. *Nat. Med.* 21: 117–119.
38. Qian, B. Z., J. Li, H. Zhang, T. Kitamura, J. Zhang, L. R. Campion, E. A. Kaiser, L. A. Snyder, and J. W. Pollard. 2011. CCL2 recruits inflammatory monocytes to facilitate breast-tumour metastasis. *Nature* 475: 222–225.
39. Germano, G., R. Frapolli, C. Belgiovine, A. Anselmo, S. Pesce, M. Liguori, E. Erba, S. Uboldi, M. Zucchetti, F. Pasqualini, et al. 2013. Role of macrophage targeting in the antitumor activity of trabectedin. *Cancer Cell* 23: 249–262.
40. Ries, C. H., M. A. Cannarile, S. Hoves, J. Benz, K. Wartha, V. Runza, F. Rey-Giraud, L. P. Pradel, F. Feuerhake, I. Klaman, et al. 2014. Targeting tumor-associated macrophages with anti-CSF-1R antibody reveals a strategy for cancer therapy. *Cancer Cell* 25: 846–859.
41. Beatty, G. L., E. G. Chiorean, M. P. Fishman, B. Saboury, U. R. Teitelbaum, W. Sun, R. D. Huhn, W. Song, D. Li, L. L. Sharp, et al. 2011. CD40 agonists alter tumor stroma and show efficacy against pancreatic carcinoma in mice and humans. *Science* 331: 1612–1616.
42. Rolny, C., M. Mazzone, S. Tugues, D. Laoui, I. Johansson, C. Coulon, M. L. Squadrito, I. Segura, X. Li, E. Knevels, et al. 2011. HRG inhibits tumor growth and metastasis by inducing macrophage polarization and vessel normalization through downregulation of PlGF. *Cancer Cell* 19: 31–44.
43. Pyonteck, S. M., L. Akkari, A. J. Schuhmacher, R. L. Bowman, L. Sevenich, D. F. Quail, O. C. Olson, M. L. Quick, J. T. Huse, V. Teijeiro, et al. 2013. CSF-1R inhibition alters macrophage polarization and blocks glioma progression. *Nat. Med.* 19: 1264–1272.
44. Rodríguez-Prados, J. C., P. G. Través, J. Cuenca, D. Rico, J. Aragonés, P. Martín-Sanz, M. Cascante, and L. Boscá. 2010. Substrate fate in activated macrophages: a comparison between innate, classic, and alternative activation. *J. Immunol.* 185: 605–614.
45. Ward, P. S., and C. B. Thompson. 2012. Metabolic reprogramming: a cancer hallmark even warburg did not anticipate. *Cancer Cell* 21: 297–308.
46. Colegio, O. R., N. Q. Chu, A. L. Szabo, T. Chu, A. M. Rhebergen, V. Jairam, N. Cyrus, C. E. Brokowski, S. C. Eisenbarth, G. M. Phillips, et al. 2014. Functional polarization of tumour-associated macrophages by tumour-derived lactic acid. *Nature* 513: 559–563.
47. Rogers, N. C., E. C. Slack, A. D. Edwards, M. A. Nolte, O. Schulz, E. Schweighoffer, D. L. Williams, S. Gordon, V. L. Tybulewicz, G. D. Brown, and C. Reis e Sousa. 2005. Syk-dependent cytokine induction by Dectin-1 reveals a novel pattern recognition pathway for C type lectins. *Immunity* 22: 507–517.
48. Underhill, D. M., E. Rossnagle, C. A. Lowell, and R. M. Simmons. 2005. Dectin-1 activates Syk tyrosine kinase in a dynamic subset of macrophages for reactive oxygen production. *Blood* 106: 2543–2550.
49. Través, P. G., P. de Atauri, S. Marín, M. Pimentel-Santillana, J. C. Rodríguez-Prados, I. Marín de Mas, V. A. Selivanov, P. Martín-Sanz, L. Boscá, and M. Cascante. 2012. Relevance of the MEK/ERK signaling pathway in the metabolism of activated macrophages: a metabolomic approach. *J. Immunol.* 188: 1402–1410.
50. LeibundGut-Landmann, S., O. Gross, M. J. Robinson, F. Osorio, E. C. Slack, S. V. Tsoni, E. Schweighoffer, V. Tybulewicz, G. D. Brown, J. Ruland, and C. Reis e Sousa. 2007. Syk- and CARD9-dependent coupling of innate immunity to the induction of T helper cells that produce interleukin 17. *Nat. Immunol.* 8: 630–638.
51. Goodridge, H. S., R. M. Simmons, and D. M. Underhill. 2007. Dectin-1 stimulation by *Candida albicans* yeast or zymosan triggers NFAT activation in macrophages and dendritic cells. *J. Immunol.* 178: 3107–3115.
52. Hsu, Y. M., Y. Zhang, Y. You, D. Wang, H. Li, O. Duramad, X. F. Qin, C. Dong, and X. Lin. 2007. The adaptor protein CARD9 is required for innate immune responses to intracellular pathogens. *Nat. Immunol.* 8: 198–205.